Food & Medicine Homology

ISSN 3006-6867 (print); 3006-4252 (online)
https://doi.org/10.26599/FMH.2026.9420097

Research Article

An efficient strategy for the rapid exploration of lipase inhibitors derived from the *Lindera aggregate* leaves by utilizing hybrid lipase-catalytic zeolitic imidazolate framework reactor combined with HPLC-Q-TOF-MS/MS and molecular docking techniques

Xin-Dan Zhang[1], Biao Liu[1], Yan-Fang Zou[1], Wen-Xiang Hu[1], Yang-Bin Lü[1], Chen-Yue Li[1], Si-Hua Quan[1], Sheng-Qiang Tong[1], Quanghuy Đoàn[2], Jing Zhao[3], Xin Peng[4] (✉), Chu Chu[1] (✉)

[1] *College of Pharmaceutical Science, Zhejiang University of Technology, Hangzhou 310014, China*
[2] *Viet Nam University of Traditional Medicine, Hà Nội 100000, Vietnam*
[3] *State Key Laboratory of Quality Research in Chinese Medicine, Macao Centre for Testing of Chinese Medicine, University of Macau, Macao 999078, China*
[4] *Ningbo Municipal Hospital of TCM, Affiliated Hospital of Zhejiang Chinese Medical University, Ningbo 315000, China*

Received: 21 September 2024 / **Revised:** 20 November 2024 / **Accepted:** 21 November 2024

Abstract: The leaves of *Lindera aggregata* (*L. aggregata*-L), which contain unspecified bioactive components, are a popular tea known for their lipid-regulating properties. This study established a novel and efficient strategy utilizing hybrid lipase–proline metal-organic framework (MOF), combined with HPLC-Q-TOF-MS/MS and molecular docking techniques, to identify potent lipase inhibitors in *L. aggregata*-L. Porcine pancreatic lipase (PPL) was immobilized within a zeolitic imidazolate framework through biomineralization, and proline was employed to enhance enzyme stability. Consequently, seven lipase inhibitors were initially identified using HPLC-Q-TOF-MS/MS and were subsequently confirmed through nuclear magnetic resonance (NMR) analysis. Their inhibitory activities were validated through an *in vitro* lipase inhibitory assay. Notably, quercetin-5-*O*-*β*-*D*-glucoside, quercetin-3-*O*-*α*-*D*-xyloside, quercetin-3-*O*-*α*-*L*-arabinofuranoside, and kaempferol-7-*O*-*α*-*L*-rhamnopyranoside were identified as novel lipase inhibitors. The mechanisms of their inhibition were preliminarily investigated through molecular docking and molecular dynamics simulations. This research provided valuable chemical insights into *L. aggregata*-L for the development of health foods and pharmaceuticals, particularly as a source of natural lipid-regulating drugs.

Keywords: *Lindera aggregata*; metal-organic framework; porcine pancreatic lipase inhibitors; molecular docking; molecular dynamics simulation

Citation: Zhang X. D., Liu B., Zou Y. F., et al. An efficient strategy for the rapid exploration of lipase inhibitors derived from the *Lindera aggregate* leaves by utilizing hybrid lipase-catalytic zeolitic imidazolate framework reactor combined with HPLC-Q-TOF-MS/MS and molecular docking techniques. *Food & Medicine Homology*, 2026, 3: 9420097. https://doi.org/10.26599/FMH.2026.9420097

1 Introduction

Herbal plant resource represents a vast chemical repository, containing a wide array of compounds that exhibit diverse bioactivities. Various constituents from these plants have been screened as lipase inhibitors with low toxicity[1-3]. Among these, *Lindera aggregata* (Sims) Kosterm. is recognized as a valuable food and pharmaceutical resource, predominantly found in the southern regions of the Yangtze River basin in China, as well as in Japan and various southeastern Asian countries[4]. Contemporary pharmacological research has demonstrated that *L. aggregata* (Sims) Kosterm possesses a broad spectrum of pharmacological properties, including anti-inflammatory, analgesic, antioxidant, and anticancer effects, as along with significant regulatory effects on the central nervous, cardiovascular, and digestive systems[5]. However, the medicinal parts of *L. aggregata* (Sims) Kosterm develop slowly, taking 8–10 years to mature, which often results in the leaves being discarded during this period and leads to inefficient resource utilization. Traditionally in China, *L. aggregata* (Sims) Kosterm leaves (*L. aggregata*-L) have been used to treat conditions such as acute cellulitis, carbuncles, gastritis, and rheumatic arthritis. Additionally, *L. aggregata*-L is commonly prepared as tea in Zhejiang province to promote liver health and reduce lipid levels. Further research has indicated that extracts from *L. aggregata*-L possess lipid-lowering properties[5,6]. However, the specific bioactive constituents of *L. aggregata*-L

© National R&D Center for Edible Fungus Processing Technology 2025. Published by Tsinghua University Press. This is an open access article under the CC BY-NC-ND license (http://creativecommons.org/licenses/by-nc-nd/4.0/).

Address correspondence to Xin Peng, pengx@nit.zju.edu.cn; Chu Chu, chuchu@zjut.edu.cn

being responsible for their lipase-inhibitory activity remain unidentified, and further scientific exploration of the underlying inhibitory mechanisms is urgently needed.

The conventional column chromatographic method for screening natural lipase inhibitors within the *Lindera* genus is characterized by low screening efficiency, complex procedures, substantial time investment and considerable costs. To data, only three flavonoids have been isolated and confirmed to exhibit lipase inhibitory activity[7]. Over the years, various strategies have been developed to expedite the screening of lipase inhibitors. Among these, ligand fishing, achieved by immobilizing target proteins on solid supports, is regarded as one of the most efficient strategies for screening active constituents due to its high efficiency and resilience to environmental stress[8,9]. In recent decades, metal-organic frameworks (MOFs) have garnered significant attention as carriers for enzyme immobilization. These frameworks consist of hybrid porous materials formed through the self-assembly of organic linkers and metal nodes via robust bonds. They offer advantages such as modifiable pore sizes, extensive surface areas, and enhanced thermal stability compared to traditional immobilization substrates[10]. MOFs have been successfully applied as carriers for the immobilization of various enzymes, including α-glucosidase, glucose oxidase, peroxidase, trypsin, and lipase[1,2,11-13]. To date, several strategies for drug screening methods based on MOF materials have been reported, including the use of UiO-66-NH_2 to screen for lipase inhibitors from *Prunella vulgaris* L.[1] and Fe_3O_4-COOH@UiO-66-NH_2 for screening lipase inhibitors in *Scutellaria baicalensis*[2]. However, challenges remain regarding the tedious synthesis processes and high costs associated with these methods. Among various MOF materials, the zeolitic imidazolate framework-8 (ZIF-8) stands out for its exceptional stability and biocompatibility, characterized by a zeolite-like crystal structure and small pore sizes[14-16]. Leveraging these properties, porcine pancreatic lipase (PPL) can be immobilized on ZIF-8 using a biomimetic mineralization approach, which significantly enhances enzyme performance after encapsulation, particularly in terms of reusability, catalytic activity, and stability[10,17]. The hybrid lipase–proline@ZIF-8 (PPL@ZIF-8) method was firstly employed to screen for natural lipase inhibitors from complex matrixes. This approach was synthetized using a simple one-pot self-assembly method, resulting in an easy experiment process and reduced costs while ensuring screening efficiency and improving the ligand fishing technologies.

This study presents a straightforward strategy for the rapid identification of lipase inhibitors derived from the industrial plant product of *L. aggregata*-L, utilizing an immobilization enzyme hybrid of lipase–catalytic ZIF-8. The specific process was illustrated in Fig. 1. PPL conjugated with suitable amino acids was firmly immobilized onto ZIF-8 using a simple one-pot self-assembly method. *p*-Nitrophenyl butyrate (*p*-NPB) was employed as the enzyme substrate, and the performance of the resulting composite was evaluated at a detection wavelength of 405 nm.

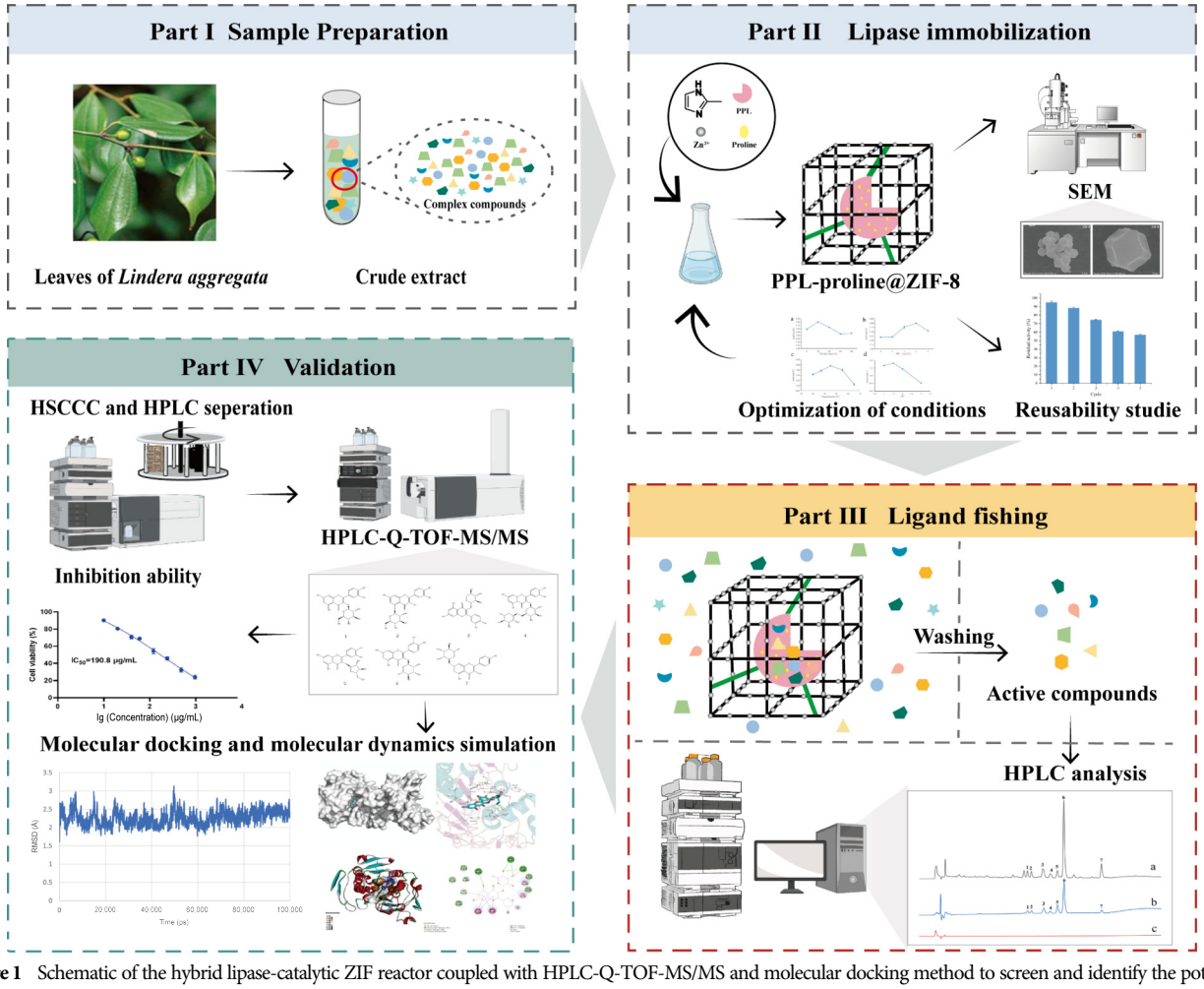

Figure 1 Schematic of the hybrid lipase-catalytic ZIF reactor coupled with HPLC-Q-TOF-MS/MS and molecular docking method to screen and identify the potential lipase inhibitors derived from *L. aggregata*-L.

Specific parameters for immobilization were optimized to enhance the immobilization efficiency. Ligand fishing of lipase inhibitors from *L. aggregata*-L was conducted on the lipase-proline@ZIF-8 (PPL@ZIF-8) system. Subsequently, the isolated compounds were preliminarily identified via high-performance liquid chromatography coupled with quadrupole-time-of-flight-mass spectrometry (HPLC-Q-TOF-MS/MS). Their structures were further confirmed through nuclear magnetic resonance (NMR) spectroscopy and compared with reference standards. The practicality and efficacy of these compounds were validated through *in vitro* inhibitory activity assays, molecular docking studies, and molecular dynamics (MD) simulations.

2 Material and methods

2.1 Materials and general instruments

The *L. aggregate*-L were provided by Zhejiang Hongshiliang Group Tiantaishan Spicebush Root Co., Ltd. (China), collected in Tiantai, Taizhou, Zhejiang Province, and authenticated by Professor Xin Peng. Orlistat, *p*-NPB were purchased from Yuanye Biotechnology Co., Ltd. (Shanghai, China). PPL was purchased from Sigma-Aldrich Co., Ltd. (Shanghai, China). Dimethyl sulfoxide (DMSO) was supplied by Xilong Scientific Co., Ltd. (Shantou, China). Sodium phosphate buffer (PBS) was supplied by Zhejiang Cienry Biotechnology Co., Ltd. (Hangzhou, China). Methanol and acetonitrile were purchased from Merck Chemicals Co., Ltd. (Beijing, Shanghai). Formic acid was obtained from Tedia Company Inc. (Fairfield, USA). Proline, zinc acetate, *p*-nitrophenol and 2-methylimidazole were purchased from Aladdin Co., Ltd. (Shanghai, China). Purified water was supplied by Hangzhou Wahaha Group (Zhejiang, China). Acetonitrile and methanol used for HPLC analysis were of chromatographic grade.

HPLC analysis was conducted using an Agilent HPLC 1260 series system (Agilent Technologies, Santa Clara, USA) equipped with an ultraviolet diode array detector of variable wavelengths (190–600 nm) and Agilent Chem Station software. Enzyme activity analysis was performed by a BioTek multi-function microplate reader. NMR data were acquired using a Bruker AVANCE III HD-600Hz Bruker AV (600 MHz for ^{1}H NMR).

2.2 Synthesis of immobilized lipase-proline@ZIF-8

The immobilization of PPL onto the MOF was carried out with specific modifications to a previously reported method[18]. Initially, lipase (3 mg/mL) and proline (20 mmol/L) were dissolved in a zinc acetate solution (40 mmol/L), to which a solution of 2-methylimidazole (160 mmol/L) was subsequently added. The resulting mixture was stirred at a speed of 200 r/min for 45 min under ambient conditions ((25 ± 2) °C). Subsequently, the white precipitate, identified as the lipase-proline MOF, was separated using refrigerated centrifugation at 9,000 r/min, followed by three washing with deionized water. The resulting precipitate was then lyophilized and utilized in subsequent experiments. For comparative purposes, a pure MOF was synthesized using the same method but without the free enzyme, this pured MOF was used for the characterization analyses. The catalytic activity of the immobilized lipase was assessed by comparing the hydrolysis of *p*-NPB with that of free lipase, as described in a previously reported spectrophotometrical method[10]. In this process, the mixture of substrate (10 mmol/L *p*-NPB) and enzyme solution (10 mg/mL) was incubated for 10 min at 37 °C, followed by centrifugation at 9,000 r/min for 3 min. The supernatant (200 μL) was then analyzed at 405 nm using a spectroscope.

2.3 Performance testing of lipase–proline@ZIF-8

2.3.1 *Enzyme loading of lipase–proline@ZIF-8*

The enzyme-loading amount on the MOF is defined as the ratio of the quantity of immobilized enzyme on the MOF to the total amount of free enzyme utilized in the immobilization procedure. This was evaluated by measuring the residual protein in the supernatant after enzyme immobilization, employing a spectroscopic method[10]. The enzyme-loading yield was estimated using the Bradford protein assay, with bovine serum albumin (1 mg/mL) serving as the protein standard. In brief, 5 mL of Coomassie Brilliant Blue G-250 solution (2 mg/mL) was mixed with 10 mL of 85% phosphoric acid, and the mixture was then diluted with water to a final volume of 100 mL. Subsequently, 3 mL of Coomassie Brilliant Blue solution was added to various concentrations of bovine serum albumin solution. The absorbance of each mixture was measured at 595 nm to establish a standard curve[10]. Using this standard curve, the protein concentration in the supernatant following enzyme immobilization was determined through identical experimental procedures. The enzyme-loading yield was calculated according to the following formula:

$$\text{Enzyme loading yield}\,(\%) = \left(\frac{A-B}{A}\right) \times 100 \qquad (1)$$

where A and B are the protein amounts of lipase in the initial solution and washing solution, respectively.

2.3.2 *Stability measurement of recycling*

The residual activity of the lipase–proline@ZIF-8 was assessed using the previously described method after storage at 4 °C for 2 weeks, allowing for an evaluation of the immobilized enzyme's longevity. The reusability of PPL@ZIF-8 was determined in accordance with methodologies reported in the literature[1]. This process involved dissolving both the substrate and the immobilized enzyme in Tris-HCl buffer, followed by incubation at 37 °C for 10 min. After centrifugation at 9,000 r/min for 3 min, the clear yellowish aqueous phase supernatant (*p*-nitrophenol) was isolated for absorbance detection at 405 nm using a BioTek multi-function microplate reader. The residual enzyme was then subjected to repeated procedures to assess the stability during recycling. The activity of freshly immobilized PPL was defined as 100%. The stability upon recycling was determined by comparing the catalytic capability of each cycle with that of the first cycle.

2.4 Measurements and characterization of lipase-proline@ZIF-8

According to the literatures, Fourier transform infrared spectroscopy (FT-IR) was employed to characterize the changes in functional groups during amidation reaction. The surfaces of ZIF-8 and lipase–proline@ZIF-8 were examined using a scanning electron microscope (SEM)[10]. Powder X-ray diffraction (XRD) patterns of pure ZIF-8 and PPL@MOF were recorded on a PANalytical Empyrean powder diffractometer in a wavelength (λ) of 0.154,1 nm Cu Kα radiation to investigate crystal structures. Additionally, thermogravimetric analysis (TGA) was used as a supplemented tool to characterize the ZIF-8 immobilized enzymes (Fig. S1)[19].

2.5 Sample preparation

In accordance with our previous study, 5 g of *L. aggregata*-L powder and 5 g of silica gel were placed in a mortar and manually blended using a pestle for 4 min to achieve a homogeneous mixture. The mixture was then quantitatively transferred to an SPE cartridge that was fitted with cotton at both ends. The absorbed analytes were eluted with 50 mL of ethanol/water solution (7:3, *V*/*V*) and subsequently concentrated under reduced pressure via a rotary evaporator[20]. The concentrated crude extract was obtained following the evaporation of the solvent.

2.6 Optimization of conditions

To enhance the screening efficiency for potential active compounds in *L. aggregata*-L extract, four critical methodological parameters were meticulously optimized: the concentration of proline and PPL, incubation temperature, and pH. The amount of enzyme required to catalyze the release of 1 mmol/L *p*-nitrophenol per minute was defined as a unit (U) of enzyme activity (initial reactive rate)[1].

2.6.1 Investigation of proline concentration

Proline was combined with PPL@ZIF-8 (5 mg) in 990 μL of PBS and 10 μL of *p*-NPB, followed by incubation at 45 °C for 10 min. The activity of the immobilized PPL was assessed using the method described in Section 2.3. The effect of varying proline concentrations (0, 20, 40, 60, 80 mmol/L) on the activity of PPL@ZIF-8 was investigated.

2.6.2 Investigation of PPL concentration

Five concentrations of PPL (0, 1, 2, 3, 4 mg/mL) were evaluated in the synthesis of PPL@ZIF-8. Following a 10 min incubation in PBS with *p*-NPB at 45 °C, the activity of each PPL@ZIF-8 formulation was determined.

2.6.3 Investigation of temperature

5 mg of PPL@ZIF-8 and 10 μL of *p*-NPB was added to PBS and incubated at various temperatures (30, 37, 45, 55, 65 °C) for 10 min. Subsequently, the activity of the immobilized enzyme was assessed.

2.6.4 Investigation of pH

In this study, 5 mg of PPL@ZIF-8 was incubated with 10 μL of *p*-NPB in 990 μL of PBS at different pH values (pH 7.0, 7.5, 8.0, 9.0) for 10 min at 45 °C. The activity of PPL@ZIF-8 was then measured accordingly.

2.7 Screening of active compounds from the crude extract

The crude extract (1 mg) of *L. aggregata*-L was dissolved in 1 mL of PBS. Subsequently, 20 mg of the PPL@ZIF-8 was added to this solution, and the mixture was incubated at 45 °C for 90 min. After incubation, this mixture was subjected to centrifugation, and the precipitate was collected and rinsed three times with 1 mL of PBS (pH 7.5) to remove non-specific constituents. To deactivate the PPL and release potential ligands, 1 mL of a 7:3 (*V*/*V*) ethanol/water solution was injected. Following a final centrifugation step, the supernatant was collected for further analysis.

2.8 Isolation of screened compounds guided by bioassay

High-speed countercurrent chromatography (HSCCC) isolation was employed to isolate four target compounds from the crude extract of *L. aggregata*-L as follows: quercetin-3-*O*-*β*-*D*-glucoside (1), quercetin-5-*O*-*β*-*D*-glucoside (2), quercetin-3-*O*-*α*-*L*-rhamnopyranoside (6), kaempferol-7-*O*-*α*-*L*-rhamnopyranoside (7), as documented in previous research[20]. The isolation procedure involved two consecutive HSCCC runs. In the first run, a solvent system comprising *n*-hexane, ethyl acetate, *n*-butanol, glacial acetic acid, water in a ratio of 2:5:2:1.5:6 (*V*/*V*) was used for isolating four compounds, including a mixture of two isomers. The second HSCCC run focused on the separation of these two isomers using a biphasic solvent system composed of ethyl acetate-*n*-butanol-0.05 mol/L of phosphate buffer (pH 3.16) containing 0.05 mol/L of hydroxypropyl-*β*-cyclodextrin in a recycling mode. Detailed HSCCC conditions were referred to the cited literature[20]. For the preparative HPLC isolation of compounds from *L. aggregata* extracts, an H&E SP-ODS-A column (250 mm × 4.6 mm, 5 μm) was utilized. Following the successful and rapid isolation of four compounds via HSCCC, preparative HPLC was employed to isolate the remaining three peaks.

The isolation was conducted using a mobile phase composed of acetonitrile (A) and water containing 0.1% formic acid (B). The gradient elution of the mobile phase was as follows: from 0 min to 20 min, 80%–70% B; from 20 min to 40 min, 70%–50% B; and from 40 min to 50 min, 50%–0% B. The flow rate of the elution was maintained at 2 mL/min, with the column temperature controlled at 30 °C. An injection volume of 100 μL was used for each run, and the eluate was monitored under 254 nm.

2.9 Identification of active compounds using HPLC-Q-TOF-MS/MS and NMR

A Kromasil 100-5 C_{18} (250 mm × 4.6 mm, 5 μm) was employed for chromatographic separation, operating at a flow rate of 1 mL/min with an injection volume of 5 μL. The column temperature was set at 30 °C. The Q-TOF-MS/MS was operated in negative ionization mode, with the following key parameters: gas temperature set to 300 °C; drying gas (nitrogen) flow rate at 10 L/min; nozzle voltage at 1 kV; capillary voltage at 3.5 kV; and fragment or voltage at 400 V. Nitrogen served as the collision gas for the MS/MS scan. HPLC was performed using an Agilent 1260 HPLC instrument. The mobile phase consisted of acetonitrile (B) and water containing 0.1% formic acid (D), with a gradient elution schedule as follows: from 0 min to 20 min, 15%–25% B; from 20 min to 30 min, 25%–50% B; from 30 min to 35 min, 50%–70% B; and from 35 min to 40 min, 70%–100% B. The flow rate was set at 1.0 mL/min, and the column temperature was maintained at 30 °C. An injection volume of 20 μL was used, and the eluate was monitored at 254 nm. Moreover, the structures of the isolated compounds were confirmed using ^{1}H NMR and compared with the reference compounds.

2.10 Lipase inhibitory activity assay

The assessment of lipase inhibitory activity, using orlistat as a positive control, was conducted with slight modifications to previous established methodologies[1,21]. PPL was dissolved in a 50 mmol/L Tris (hydroxymethyl) aminomethane (Tris)-HCl buffer (pH 8.0), yielding a final enzyme concentration of 1 mg/mL. Each isolated compound was dissolved in 1 mL of DMSO and then diluted with 24 mL of 13 mmol/L Tris-HCl buffer (pH 8.0) to achieve various sample concentrations. Subsequently, 50 μL of 0.1 mmol/L solution of 4-methylumbelliferone oleate (4-MU), prepared in a 13 mmol/L

Tris-HCl buffer, was added to each well of a 96-well microtiter plate. The enzymatic reaction was initiated by the addition of 25 μL of the lipase solution. After a 30 min incubation period at 25 °C, sodium citrate was used to terminate the reaction. The release of 4-MU was quantified using a fluorometric microplate reader, with an excitation wavelength of 355 nm and an emission wavelength of 460 nm. All measurements were conducted in triplicate, and the results were expressed as the mean ± standard deviation (SD) according to the following equation:

$$\text{Inhibition activity}(\%) = \left(1 - \frac{A_{\text{Sample}} - A_{\text{Sampleblank}}}{A_{\text{Control}} - A_{\text{Controlblank}}}\right) \times 100 \quad (2)$$

where A_{Sample}, $A_{\text{Sampleblank}}$, A_{Control}, and $A_{\text{Controlblank}}$ were absorbances of the tested sample, blank sample, control and blank control, respectively. The half-maximal inhibitory concentration (IC_{50}) of the screened compounds were calculated by Graphpad Prism (version 8.0.2) after providing inhibition activity and the corresponding concentration.

2.11 Molecular docking

Molecular docking simulations between lipase and active compounds were performed using Autodock 3.7.5 software to further analyze their specific interactions[2,21,22]. The crystal structure of PPL was obtained from RCSB protein database (http://www.rcsb.org/) with PDB ID 1ETH[21,22]. PyMOL (version 1.5.7) was utilized to remove co-crystalline ligands and water molecules from the lipase structure, followed by the addition of nonpolar hydrogen and charges using AutoDockTools (version 2.4.0). Docking parameters were configured to encompass the active sites of lipase within a grid box, thereby facilitating the identification of the active site. Subsequently, automatic molecular docking was conducted using AutoDock Vina (version 1.1.2) to obtain optimal results. In line with previous studies[23], the grid size (xyz point) was set to dimensions of 60 × 60 × 60 and the center was set to 54.015, 47.006, and 123.000, while all other parameters was default. The resulting molecular conformations of various flavonoids docked onto the PPL crystal structure were visualized using Discovery Studio 2021[21].

2.12 MD simulation

The AMBER18 software package was used for MD simulation to evaluate the interactions and binding stability between lipase and screened potential lipase inhibitors. The protein systems were parameterized using the FF14Sb force field, while the ligands were processed using the GAFF force field. Atomic charges were calculated using AM1-BCC implemented in the ANTECHAMBER module.

The protein was prepared in the tleap utility, which automatically added hydrogen atoms and counterions to neutralize the charge. The TIP3P water model was utilized to solvate each complex. To initiate the MD simulations, the protein-ligand complexes underwent a preliminary process that included energy minimization of water molecules for 10,000 steps at a constant number of atoms. The system temperature was then increased to 300 K over a period of 50 ps, followed by 100 ns of MD simulations in the NPT ensemble. The dynamics and interactions of the protein-ligand complexes were analyzed using the CPPTRAJ module. Additionally, the MMPBSA.py module was employed to calculate the binding free energy between the ligands and proteins.

3 Results and discussion

3.1 Characterization of the ZIF-8 and the lipase–proline@ZIF-8

The structural alterations induced by the incorporation of proline into PPL were confirmed through FT-IR spectroscopy. The spectra for free PPL (a), PPL@ZIF-8 (b), and proline@ZIF-8 (c) were presented in Fig. 2A. Notable absorption peaks around 425 cm^{-1} were observed in both Fig. 2A(b) and (c), indicating the characteristics of the Zn-N vibration band associated with ZIF-8. Additionally, characteristic bands emerging at 995 and 2,927 cm^{-1} corresponded to the in-plane bending vibrations of the imidazolate ring and asymmetric aliphatic and aromatic C–H vibrations of 2-methylimizdazole, which were consistent with the reported ZIF-8 structure[18]. The successful entrapment of lipase–proline within ZIF-8 via biomineralization was confirmed by the emergence of amide bands at 1,637 and 1,617 cm^{-1} [10].The XRD profile presented in Fig. 2B was utilized to assess the crystallinity of MOF before and after immobilization. Characteristic peaks at 2θ values of 7.29°, 10.34°, 12.72°, 14.67°, 16.43°, 18.03°, 22.07°, 24.54°, 26.77°, 29.57° were observed for pure ZIF-8, which closely resembled those of PPL@ZIF-8. This similarity indicates that the crystalline structure and the physicochemical properties of ZIF-8 remained unchanged after the incorporation of lipase[18]. The structure and morphologies of the ZIF-8 and PPL@ZIF-8 were further illustrated using SEM. As shown in Fig. 2C, the ZIF-8 particles exhibit a loosely arranged, regular cubic structure characterized by a smooth surface and multiple cavities. In contrast, the SEM image of the PPL@ZIF-8 displayed a distinct morphological transformation, characterized by a larger surface area and clusters forming irregular shapes. This change may be attributed to the enzyme acting as nucleation sites, facilitating the formation of a protective framework that encapsulates the enzyme within the MOF. The successful synthesis of the PPL@ZIF-8 was further corroborated by the observed morphological differences in the SEM images[10].

3.2 Enzyme loading and recycling stability of lipase–proline@ZIF-8

Following the immobilization of PPL onto the ZIF-8, the enzyme-loading efficiency was determined by measuring the residual protein concentration in the supernatant. Among the synthesized composites, an impressive loading efficiency of 92.63% was achieved.

The biocatalyst serves as a key determinant of economic viability, thus, the reusability of the PPL@ZIF-8 was evaluated by examining the residual activities after multiple cycles under optimal condition. As shown in Fig. 3, the immobilized lipase maintained a high level of relative enzymatic activity following the first reaction cycle. Notably, more than 50% of the initial activity of PPL@ZIF-8 was retained after five cycles of reuse, indicating that the bond between the enzyme and carrier was effectively strengthened by immobilization. This enhancement was beneficial for improving enzyme stability and reducing enzyme consumption[24]. The observed decline in enzymatic activity beyond five cycles might be attributed to several factors. One possible reason for this phenomenon is the accumulation of enzyme inhibitors resulting from the enzymatic process, which can create an inhibitory microenvironment around the enzyme. Additionally, the loss of particles, enzyme deactivation or

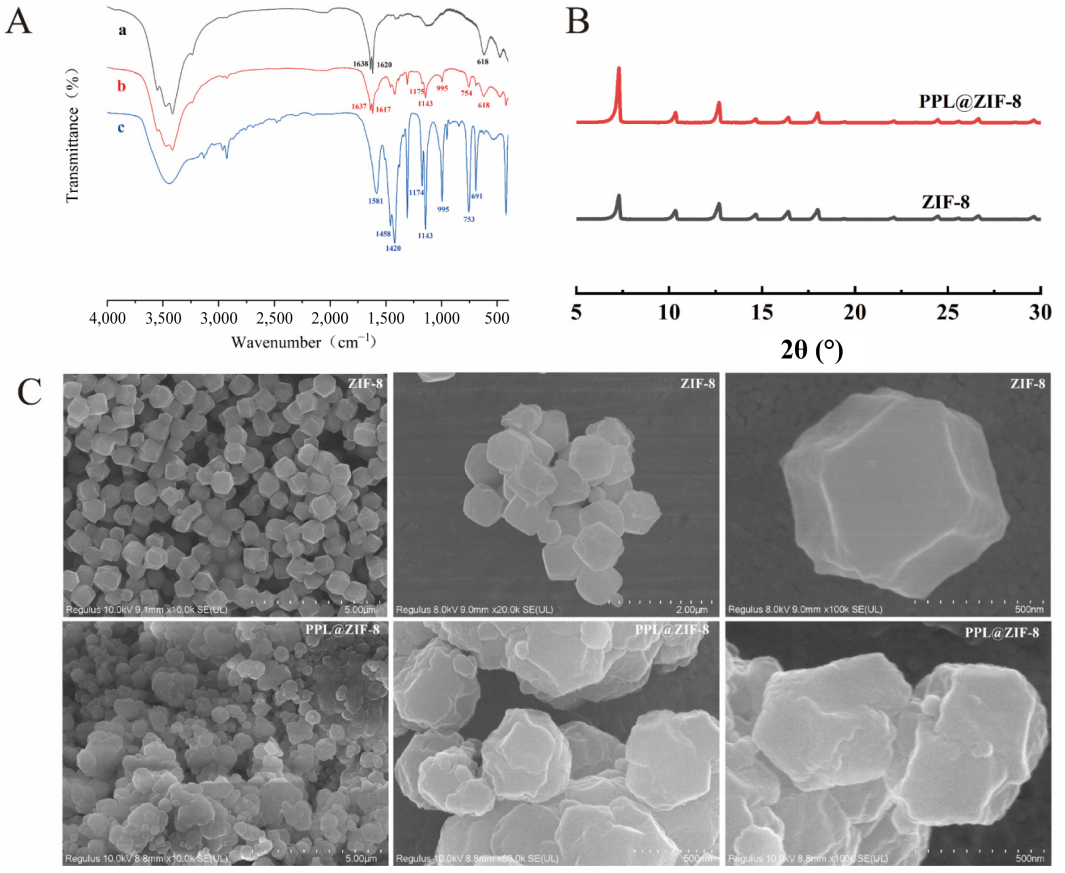

Figure 2 Characterization of the ZIF-8 and the lipase-proline@ZIF-8. (A) FT-IR spectra of free PPL (a), lipase-proline@ZIF-8 (b), proline@ZIF-8 (c). (B) PXRD patterns of ZIF-8 and lipase–proline@ZIF-8. (C) SEM images of ZIF-8 and lipase–proline@ZIF-8 under different magnification (the magnification displayed in each image).

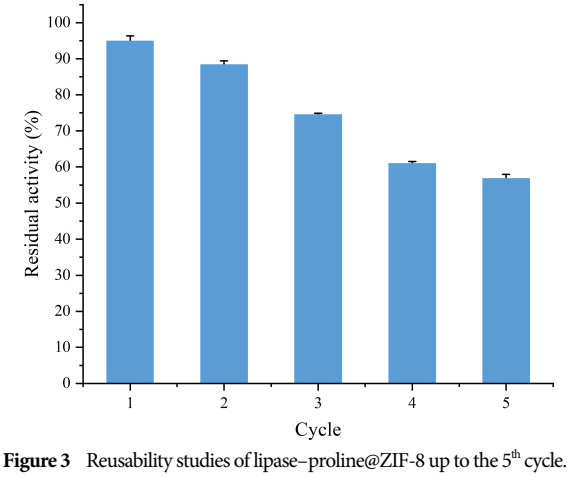

Figure 3 Reusability studies of lipase–proline@ZIF-8 up to the 5th cycle.

mechanical damage of PPL@ZIF-8 during the reuse experiments may also contribute to the decreased activity[18].

3.3 Optimal parameters

3.3.1 *Investigation of proline concentration for ZIF-8*

Proline is known for its high solubility among amino acid, which can prevent gathering during the refolding process and lead to the formation of loose aggregates at higher concentrations[25]. This occurs due to interactions with the folding intermediate that retain protein inactivity. As depicted in Fig. 4A, 20 mmol/L was identified as the optimal level of proline for maximizing lipase activity. Beyond this concentration, a decline in enzyme activity was observed, which may attributed to the formation of a more compact protein structure induced by higher proline concentrations[25].

3.3.2 *Investigation of the lipase concentration for ZIF-8*

The effect of enzyme concentration on the activity of PPL@ZIF-8 was examined by varying the concentration of PPL@ZIF-8. As demonstrated in Fig. 4B, the relative activity of the immobilized lipase increased up to a concentration of 3 mg/mL. However, besides this concentration, a decline in activity was observed. This trend may be probably attributed to the reduced space gap between enzyme molecules at higher concentrations, which disrupts the interaction between the enzyme's active site and substrate molecules, leading to excessive enzyme aggregation[2,26]. Furthermore, the likelihood of interactions between the enzyme and adjacent protein molecules increases with higher protein concentration, potentially causing structural distortion and enzyme denaturation[27].

3.3.3 *Investigation of temperature for lipase–proline@ZIF-8*

To evaluate the thermal stability of immobilized enzyme and its effect on the efficiency of enzyme catalytic efficiency, PPL@ZIF-8 was incubated with *p*-NPB at various temperatures ranging from 30 °C to 65 °C. As shown in Fig. 4C, the relative activity of the PPL@ZIF-8 increased with temperature, reaching a maximum at 45 °C. However, the activity of PPL@ZIF-8 dramatically decreased when the temperature exceeded 55 °C. This reduction in activity at elevated temperatures can be ascribed to the disruption of

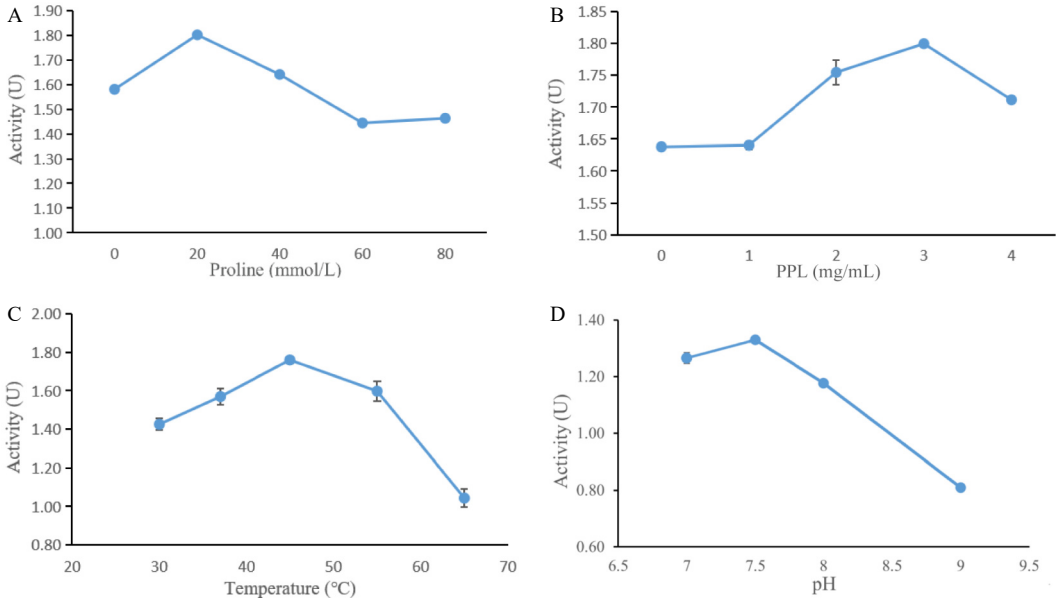

Figure 4 Effects of proline concentration (A), PPL concentration (B), temperature (C), pH (D) on the relative activity of lipase-proline@ZIF-8.

non-covalent interactions within the enzyme and the alteration in its conformation or active site[28].

3.3.4 Investigation of pH for the lipase–proline@ZIF-8

The activity of the immobilized enzyme is typically sensitive to the pH of their environment. In this study, PPL@ZIF-8 was incubated with *p*-NPB in PBS across a range of alkaline conditions (pH 7.0–9.0) for 10 min at 45 °C, followed by the assessment of enzyme activity. As illustrated in Fig. 4D, the relative activity of PPL@ZIF-8 exhibited an upward trend as the pH increased from 7.0 to 7.5, primarily due to the conformational stabilization of lipase–proline molecules on ZIF-8[17]. However, the activity of lipase–proline MOF rapidly declined when the pH exceeded 7.5, suggesting that the dissociation state and behavior of the enzyme were affected by the acidic and alkaline environment[27].

3.4 Screening of potential lipase inhibitors by lipase–proline@ZIF-8 and identification of screened compounds

The established method was applied to fish out potential PPL inhibitors from *L. aggregata*-L. Three fractions were analyzed in sequence: the crude extract of *L. aggregata*-L, the elution of the ligand fishing assay by PPL@ZIF-8, and the third time PBS washing solution following the ligand fishing assay using PPL@ZIF-8. These fractions were assessed by HPLC-Q-TOF-MS/MS. As displayed in Fig. 5, no compound was detected in Fig. 5(c), indicating that all non-specific binding constituents had been effectively removed. In comparison to Fig. 5(a), the non-specific binding constituents disappeared and the peak areas of overloaded specific binding constituents decreased in Fig. 5(b). Consequently, seven compounds were identified as potential PPL inhibitors in Fig. 5(b).

The screened compounds were bio-guided, separated and initially characterized based on their retention times and fragmentation patterns by referencing the relevant literature. Subsequently, their structures were confirmed through NMR analysis and comparison with reference compounds. As demonstrated in Table S1, the same fragment ions at *m/z* 301 were exhibited in compounds 1–6, indicating the presence of a quercetin base structure[29]. The molecular ion peak of compound

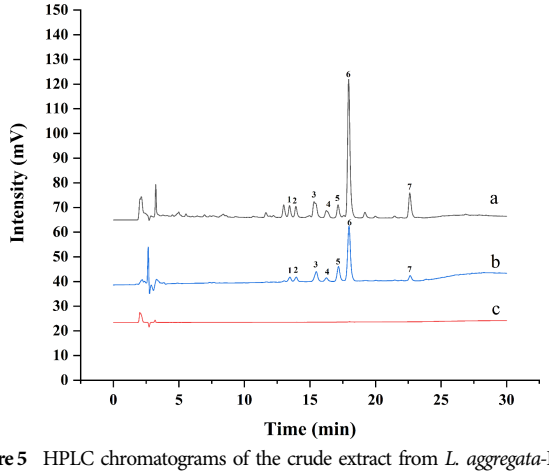

Figure 5 HPLC chromatograms of the crude extract from *L. aggregata*-L (a), the lipase inhibitor screened by lipase–proline@ZIF-8 (b), the third PBS washing solution (c).

1 at *m/z* 463.114,8 was observed with a fragment ion peak at *m/z* 301.029,1 $[M-H-162]^-$ associated with the loss of a glucose molecule. The ions at *m/z* 271.021,1 $[M-H-146-30]^-$ and *m/z* 255.031,6 $[M-H-146-30-16]^-$ were caused by the loss of CH_2O and O, respectively. The ion at *m/z* 151.005,6 was generated following a Retro-Diels Alder (RDA) cleavage[30]. The $[M-H]^-$ ion of compound 2 at *m/z* 463.089,1 exhibited fragmentation patterns similar those of compound 1. Compounds 3 and 5 both possessed a molecular weight of 433 and were further fragmented to yield the characteristic ions at *m/z* 301 and 255. However, in the MS spectrum of compound 3, the fragment ion at *m/z* 371.061,1 $[M-H-62]^-$ was generated from the loss of CO_2 and H_2O, indicating that this compound was quercetin-3-*O*-*α*-*D*-xyloside (3).

Consequently, compound 5 was identified as quercetin-3-*O*-*α*-*L*-arabinofuranoside (5)[31]. Compound 4 was identified as quercetin-3-*O*-rutinoside, with the $[M-H]^-$ ion at *m/z* 609.143,6 and the main fragment ions at *m/z* 301.021,9 and 151.001,4[30]. In the MS spectrum of compound 6, ions of $[M-H-146]^-$ at *m/z* 301.034,2 were detected, which were the characteristic ions of the rhamnopyranoside unit. Similar to compound 1, ions were generated at *m/z* 271.024,1 $[M-H-146-30]^-$ and *m/z* 255.029,5

$[M-H-146-30-16]^-$ due to the loss of CH_2O and O, respectively. Thus, this compound can be deduced to be quercetin-3-*O*-*α*-*L*-rhamnopyranoside (6) ($C_{21}H_{20}O_{11}$). Based on the main fragment ion at *m/z* 285.040,0 $[M-H-146]^-$ (Fig. S2) and the molecular ion peak at *m/z* 431.101,7 $[M-H]^-$ obtained from the MS spectrum, compound 7 was identified as kaempferol-7-*O*-*α*-*L*-rhamnopyranoside (7). Following the bio-assay guided isolation described in Section 2.8, seven compounds were successfully obtained. Among them, four compounds—quercetin-3-*O*-*β*-*D*-glucoside (1), quercetin-5-*O*-*β*-*D*-glucoside (2), quercetin-3-*O*-*α*-*L*-rhamnopyranoside (6), and kaempferol-7-*O*-*α*-*L*-rhamnopyranoside (7)) were effectively separated by magnified MPSD extraction combined with HSCCC isolation. Their structures were confirmed by MS and NMR analyses, as detailed in our published paper[20]. The remaining three screened inhibitors were isolated using preparative HPLC and identified through comparison with reference compounds. The specific structures of these compounds were shown in Fig. S3.

3.5 Validation of pancreatic lipase inhibitory activity of the seven compounds

In this study, the inhibitory effects of seven target compounds were evaluated *in vitro*, with orlistat serving as the positive control. The results of the assay were presented in Table 1. Compared to the IC_{50} value of (0.15 ± 0.02) μmol/L for orlistat, moderate lipase inhibitory activity was observed in quercetin-3-*O*-*α*-*L*-rhamnopyranoside (6) and kaempferol-7-*O*-*α*-*L*-rhamnopyranoside (7), with calculated IC_{50} values of (78.97 ± 6.05) and (98.36 ± 27.73) μmol/L, respectively. In contrast, compared with the rhamnoside glycosides, weaker inhibitory effects were observed for quercetin-3-*O*-*β*-*D*-glucoside, quercetin-3-*O*-*α*-*D*-xyloside, quercetin-3-*O*-rutinoside, and quercetin-3-*O*-*α*-*L*-arabinofuranoside, which exhibited IC_{50} values of (228.90 ± 12.50), (167.70 ± 34.08), (165.00 ± 14.95), and (217.70 ± 58.23) μmol/L, respectively. Notably, quercetin-5-*O*-*β*-*D*-glucoside, an isomer of quercetin-3-*O*-*β*-*D*-glucoside, demonstrated a significantly weaker inhibitory effect, with an IC_{50} value of (1,425.64 ± 19.62) μmol/L. These findings highlighted the need for further investigation into the structure-effect relationship of these compounds.

3.6 Molecular docking study

Molecular docking simulations were conducted to elucidate the binding conformations and preferred binding sites of seven potential hypolipidemic active compounds combined with lipase, aiming to explaining their interaction mechanisms[21]. As shown in Table 2, the binding free energy between orlistat and lipase was −7.1 kcal/mol. In contrast, the seven compounds exhibited remarkable binding free energies of −9.4, −8.9, −9.8, −9.3, −9.2, −9.1, and −9.8 kcal/mol, respectively. When compared to recently reported compounds with potent lipase inhibitory activities, such as tetrahydromethoxychalcone, licochalcone B, echinatin, isoliquiritigenin, licochalcone D, licochalcone E, licochalcone A, which displayed binding energies of −8.6, −8.8, −8.5, −8.7, −9.6, −9.3, −9.3 kcal/mol, respectively[32], the screened compounds demonstrated strong affinity for PPL, suggesting their ease of binding with the enzyme[33]. Furthermore, the interactions between the compounds derived from *L. aggregata*-L were elucidated through molecular docking, as illustrated in Fig. S4. Each ligand interacted with the amino acid residues surrounding the active site of lipase via hydrogen bonds and alkyl interactions, thereby enhancing the stability of the ligand–lipase complex[34]. The specific residues that interacted with each potential inhibitor were shown as Table 2, which directly indicates the potential PPL inhibitory activities of the screened compounds. According toa previous study[23], the catalytic activity of pancreatic lipase was closely related to the amino acid residues SER153 and HIS264. Compounds 3–7 established strong hydrophobic interactions with lipase through the amino acid residues HIS264, PHE216, TYR115, and PHE78. The inhibitory effects of compounds 1 and 2 were depended on the formation of hydrophobic interactions with the amino acid residues ILE79 and PHE78, as well as the establishment of hydrogen bonds with ASP80[22, 34].

3.7 MD simulations study

A MD study was conducted to validate the results of molecular docking and to assess the stability and interactions between PPL and small molecule ligands[35]. Based on the interactions with the binding pocket, PPL inhibitory activity, and calculated binding energies (Figs. 6A-6D, S4, and Tables 1, 2), the docked complexes of compounds 1, 2, 6, and 7 were selected for MD simulations. To evaluate stability, the root-mean-square deviation (RMSD) of the initial structures was calculated over a period of 100 ns was calculated. The average RMSDs values were determined to be 2–3 Å for the compound 1-PPL complex (Fig. 6E), 2–2.5 Å for the compound 2-PPL complex (Fig. 6F), 2–3 Å for the compound 6-PPL complex (Fig. 6G), and 3–4 Å for the compound 7-PPL complex (Fig. 6H). The affinity of the ligand for its target can be reflected in the binding free energy (ΔG_{bind}). The MM-GBSA method implemented in Ambertools 18 was used to calculate ΔG_{bind} for the four compound-lipase complexes. The results were presented in Table 3, where the ΔG_{bind} values of compounds 1, 2, 6, and 7 were found to be −30, −26, −35, and −24 kcal/mol, respectively.

The analysis of protein-ligand interactions plays a crucial role in identifying target sites. Hydrogen bond is essential for maintaining the stability of docking complexes. During the MD simulations, the compound 1-PPL complex formed hydrogen bonds with

Table 1 *In vitro* PPL inhibitory activity of the seven compounds screened by lipase-proline MOF coupled with HPLC-Q-TOF-MS/MS

Peak	Compounds	IC_{50} (μmol/L)
1	Quercetin-3-*O*-*β*-*D*-glucoside (isoquercitrin)	228.90 ± 12.50
2	Quercetin-5-*O*-*β*-*D*-glucoside	1,425.64 ± 19.62
3	Quercetin-3-*O*-*α*-*D*-xyloside (reynoutrin)	167.70 ± 34.08
4	Quercetin-3-*O*-rutinoside (rutin)	165.00 ± 14.95
5	Quercetin-3-*O*-*α*-*L*-arabinofuranoside(avicularin)	217.70 ± 58.23
6	Quercetin-3-*O*-*α*-*L*-rhamnopyranoside (quercitrin)	78.97 ± 6.05
7	Kaempferol-7-*O*-*α*-*L*-rhamnopyranoside	98.36 ± 27.73
Positive control	Orlistat	0.15 ± 0.02

Table 2 Results of molecular docking analysis of seven compounds

Compounds	Binding energy (kcal/mol)	Interaction residues
Quercetin-3-*O*-*β*-*D*-glucoside (isoquercitrin)	−9.4	ASP80, PHE78, VAL260, ILE79
Quercetin-5-*O*-*β*-*D*-glucoside	−8.9	PHE216, PHE78, ASP80, ALA261, ILE79, TYR115
Quercetin-3-*O*-*α*-*D*-xyloside (reynoutrin)	−9.8	HIS152, ALA261, HIS264, TYR115, PHE216, PHE78
Quercetin-3-*O*-rutinoside (rutin)	−9.3	ASP80, TRP253, ALA261, PHE78, PHE216, TYR115, HIS264
Quercetin-3-*O*-*α*-*L*-arabinofuranoside (avicularin)	−9.2	SER153, PHE 78, TYR115, PHE216, ILE79, VAL260
Quercetin-3-*O*-*α*-*L*-rhamnopyranoside (quercitrin)	−9.1	PHE216, PHE78, TYR115, ALA261, VAL260, HIS264
Kaempferol-7-*O*-*α*-*L*-rhamnopyranoside	−9.8	HIS264, TYR 115, ARG257, PHE216, PHE78, ALA261, VAL260
Orlistat	−7.1	GLY77, PHE78, HIS152, HIS264, ASP80, LEU265, TYR115, PRO181, ALA261, PHE216, ILE79, ILE210, VAL260

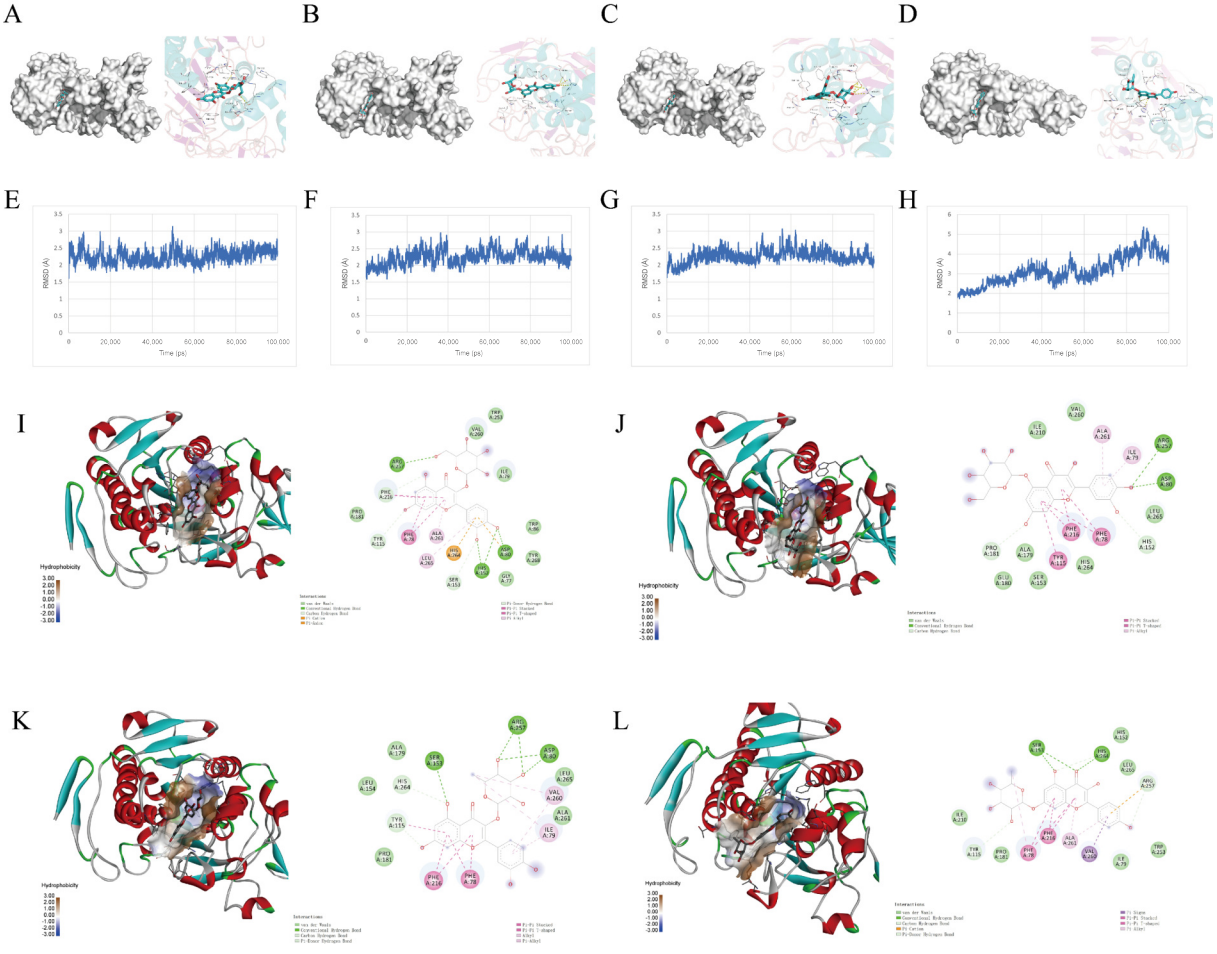

Figure 6 Docking complexes in active pocket site of PPL and MD simulation results: (A) PPL-quercetin-3-*O*-*β*-*D*-glucoside complex; (B) PPL-quercetin-5-*O*-*β*-*D*-glucoside complex; (C) PPL-quercetin-3-*O*-*α*-*L*-rhamnopyranoside complex; (D) PPL-kaempferol-7-*O*-*α*-*L*-rhamnopyranoside complex; (E) RMSD of PPL-quercetin-3-*O*-*β*-*D*-glucoside; (F) RMSD of PPL-quercetin-5-*O*-*β*-*D*-glucoside; (G) RMSD of PPL-quercetin-3-*O*-*α*-*L*-rhamnopyranoside; (H) RMSD of PPL-kaempferol-7-*O*-*α*-*L*-rhamnopyranoside; (I) amino acid interactions of quercetin-3-*O*-*β*-*D*-glucoside (1); (J) amino acid interactions of quercetin-5-*O*-*β*-*D*-glucoside (2); (K) amino acid interactions of quercetin-3-*O*-*α*-*L*-rhamnopyranoside (6); (L) amino acid interactions of kaempferol-7-*O*-*α*-*L*-rhamnopyranoside (7).

ASP80 and HIS152, and also engaged in pi-pi stacking interactions with PHE78 (Fig. 6I). In the compound 2-PPL complex, two hydrogen bonds were observed, one between ASP80 and an OH group, and another between ARG257 and an OH group. Additionally, pi-pi interactions were formed between the benzene ring of compound 2 and PHE216, PHE78, and TYR115 (Fig. 6J). In the compound 6-PPL complex, hydrogen bonds were detected between the OH group of the compound 6 and the SER153 and ARG257 residues of PPL, along with pi-pi stacking involving the benzene ring, PHE216, and PHE78 (Fig. 6K). The compound 7-PPL complex exhibited two hydrogen bonds: one involving SER153 and an OH group, and the other involving

Table 3 Binding free energy of compound 1, 2, 6, 7 using MM-GBSA method

Compounds	Binding energy (kcal/mol)
Quercetin-3-*O*-*β*-*D*-glucoside (isoquercitrin)	−30
Quercetin-5-*O*-*β*-*D*-glucoside	−26
Quercetin-3-*O*-*α*-*L*-rhamnopyranoside (quercitrin)	−35
Kaempferol-7-*O*-*α*-*L*-rhamnopyranoside	−24

HIS264 and a carbonyl (C=O) group (Fig. 6L). Overall, the effectiveness of the docking results was validated, with no detectable effects of temperature and pressure on structural conformations.

4 Conclusions

In this study, PPL@ZIF-8, a novel hybrid lipase–catalytic ZIF reactor, was successfully developed for the effective screening of PPL inhibitor derived from *L. aggregata*-L. This reactor exhibited enhanced recyclability of PPL as well as superior storage stability and thermal stability, thereby significantly broadening the application of enzymes during the screening process. Based on this, an efficient and reliable method that integrates PPL@ZIF-8 with HPLC-Q-TOF-MS/MS was established to screen bioactive compounds from the industrial plant of *L. aggregata*. As expected, seven potential PPL inhibitors were identified, including the first reported lipase inhibitory compounds: quercetin-5-*O*-*β*-*D*-glucoside (2), quercetin-3-*O*-*α*-*D*-xyloside (3), quercetin-3-*O*-*α*-*L*-arabinofuranoside (5), and kaempferol-7-*O*-*α*-*L*-rhamnopyranoside (7). The potential inhibition mechanisms of these bioactive compounds were studied and validated through molecular docking and MD simulation. The action mechanism of *L.aggregata*-L about lipase inhibitory would be elucidated in further pharmacological research conducted within a more comprehensive clinical manner. In summary, this innovative approach provides a valuable reference for the identification of potential functional compounds in a variety of natural products. Importantly, this study establishes a chemical foundation for future exploration and utilization of *L. aggregata*-L in the health food and pharmaceutical industries, particularly in management and alleviation of blood lipid levels.

Conflicts of interest

The authors declare that there are no conflicts of interest in this work.

Acknowledgments

This study was supported by the National Natural Science Foundation of China (No. 82374017, 82073979), The Major Science and Technology Projects of Breeding New Varieties of Agriculture in Zhejiang Province (No. 2021C02074), and Ningbo Top Medical and Health Research Program (No. 2022030309). Besides, the authors acknowledge support from Zhejiang Provincial Key Laboratory of TCM for Innovative R & D and Digital Intelligent Manufacturing of TCM Great Health Products, and appreciate for English polishing from Professor Dai Wenting.

Electronic Supplementary Material (ESM)

The online version contains supplementary material available at https://doi.org/10.26599/ FMH.2026.9420097.

References

[1] Chen, X. L., Xue, S., Lin, Y. L., et al. Immobilization of porcine pancreatic lipase onto a metal-organic framework, PPL@MOF: a new platform for efficient ligand discovery from natural herbs. *Analytica Chimica Acta*, **2020**, 1099: 94–102. https://doi.org/10.1016/j.aca.2019.11.042

[2] Xu, J. F., Cao, P. K., Fan, Z. Y., et al. Rapid screening of lipase inhibitors in *Scutellaria baicalensis* by using porcine pancreatic lipase immobilized on magnetic core–shell metal–organic frameworks. *Molecules*, **2022**, 27: 3475. https://doi.org/10.3390/molecules27113475

[3] Mei, J., Guo, R. L., Zhang, F., et al. Identification of bioactive natural products using yeast: application to monoacylglycerol lipase inhibitor extraction from Corydalis Rhizoma. *Biomedicine & Pharmacotherapy*, **2022**, 149: 112798. https://doi.org/10.1016/j.biopha.2022.112798

[4] Wang, J., Wang, F. R., Yuan, L. X., et al. Aqueous extracts of *Lindera aggregate* (Sims) Kosterm leaves regulate serum/hepatic lipid and liver function in normal and hypercholesterolemic mice. *Journal of Pharmacological Sciences*, **2020**, 143: 45–51. https://doi.org/10.1016/j.jphs.2020.01.009

[5] Sun, C. L., Yu, S. L., Li, S. M., et al. Chemical constituents from the leaves of *Lindera aggregata*. *Chinese Traditional Patent Medicine*, **2022**, 44: 464–469. https://doi.org/10.3969/i.issn.1001-1528.2022.02.024

[6] Lü, Y. B., Zou, Y. F., Zhang, X. D., et al. A review on the chemical constituents and pharmacological efficacies of *Lindera aggregata* (Sims) Kosterm. *Frontiers in Nutrition*, **2022**, 9: 1071276. https://doi.org/10.3389/fnut.2022.1071276

[7] Devkota, A. A., Dirar, A. I., Kurizaki, A., et al. Extraction and isolation of kaempferol glycosides from the leaves and twigs of *Lindera neesiana*. *Separations*, **2019**, 6: 10. https://doi.org/10.3390/separations6010010

[8] Xie, L. L., Lee, D. Y., Shang, Y., et al. Characterization of spirostanol glycosides and furostanol glycosides from anemarrhenae rhizoma as dual targeted inhibitors of 5-lipoxygenase and cyclooxygenase-2 by employing a combination of affinity ultrafiltration and HPLC/MS. *Phytomedicine*, **2020**, 77: 153284. https://doi.org/10.1016/j.phymed.2020.153284

[9] Li, S. L., Wang, R. M., Hu, X. P., et al. Bio-affinity ultra-filtration combined with HPLC-ESI-qTOF-MS/MS for screening potential *α*-glucosidase inhibitors from *Cerasus humilis* (Bge.) Sok. leaf-tea and *in silico* analysis. *Food Chemistry*, **2022**, 373: 131528. https://doi.org/10.1016/j.foodchem.2021.131528

[10] Vaidya, L. B., Nadar, S. S., Rathod, V. K. Entrapment of surfactant modified lipase within zeolitic imidazolate framework (ZIF)-8. *International Journal of Biological Macromolecules*, **2020**, 146: 678–686. https://doi.org/10.1016/j.ijbiomac.2019.12.164

[11] Wang, S., Wang, Y. X., Wang, S. X., et al. Lipase immobilization on multi-walled carbon nanotubes used as a target fishing tool and followed by molecular docking technique to analyze lipase inhibitor from *Robinia pseudoacacia* L. *Industrial Crops and Products*, **2022**, 178: 114645. https://doi.org/10.1016/j.indcrop.2022.114645

[12] Hu, Y. L., Dai, L. M., Liu, D. H., et al. Rationally designing hydrophobic UiO-66 support for the enhanced enzymatic performance of immobilized lipase. *Green Chemistry*, **2018**, 20: 4500–4506. https://doi.org/10.1039/C8GC01284A

[13] Zhong, Y. Y., Yu, L. J., He, Q. Y., et al. Bifunctional hybrid enzyme-catalytic metal organic framework reactors for *α*-glucosidase inhibitor screening. *ACS Applied Materials and Interfaces*, **2019**, 11: 32769–32777. https://doi.org/10.1021/acsami.9b11754

[14] Ji, Y., Wu, Z. Z., Zhang, P., et al. Enzyme-functionalized magnetic framework composite fabricated by one-pot encapsulation of lipase and Fe_3O_4 nanoparticle into metal–organic framework. *Biochemical Engineering Journal*, **2021**, 169: 107962. https://doi.org/10.1016/j.bej.2021.107962

[15] Ozyilmaz, E., Ascioglu, S., Yilmaz, M. Calix[4]arene tetracarboxylic acid-treated lipase immobilized onto metal-organic framework: biocatalyst for ester hydrolysis and kinetic resolution. *International Journal of Biological Macromolecules*, **2021**, 175: 79–86. https://doi.org/10.1016/j.ijbiomac.2021.02.003

[16] Lyu, F. J., Zhang, Y. F., Zare, R. N., et al. One-Pot synthesis of protein-embedded metal–organic frameworks with enhanced biological activities. *Nano Letters*, **2014**, 14: 5761–5765. https://doi.org/10.1021/nl5026419

[17] He, H. M., Han, H. B., Shi, H., et al. Construction of thermophilic

lipase-embedded metal–organic frameworks via biomimetic mineralization: a biocatalyst for ester hydrolysis and kinetic resolution. *ACS Applied Materials and Interfaces*, **2016**, 8: 24517–24524. https://doi.org/10.1021/acsami.6b05538

[18] Nadar, S. S., Rathod, V. K. Immobilization of proline activated lipase within metal organic framework (MOF). *International Journal of Biological Macromolecules*, **2020**, 152: 1108–1112. https://doi.org/10.1016/j.ijbiomac.2019.10.199

[19] Lázaro, I. A. A comprehensive thermogravimetric analysis multifaceted method for the exact determination of the composition of multifunctional metal-organic framework materials. *European Journal of Inorganic Chemistry*, **2020**: 4284–4294. https://doi.org/10.1002/ejic.202000656

[20] Zou, Y. F., Lü, Y. B., Peng, X., et al. A novel strategy by combining "magnified" matrix solid phase dispersion extraction with high-speed countercurrent chromatography for the rapid and efficient isolation of flavonoids isomers with anti-inflammatory effect from *Lindera aggregata* (Sims) Kosterm leaves. *Sustainable Chemistry and Pharmacy*, **2023**, 33: 101073. https://doi.org/10.1016/j.scp.2023.101073

[21] Jin, P. Y., Chen, L. Z., Zhong, J. J., et al. Screening and identification of lipase inhibitors extracted from *Dioscorea nipponica* Makino by UV–vis and HPLC coupled to UPLC-Q-TOF-MS/MS. *International Journal of Biological Macromolecules*, **2023**, 230: 123427. https://doi.org/10.1016/j.ijbiomac.2023.123427

[22] Hu, J. F., Wang, H. Y., Weng, N. H., et al. Novel angiotensin-converting enzyme and pancreatic lipase oligopeptide inhibitors from fermented rice bran. *Frontiers in Nutrition*, **2022**, 9: 1010005. https://doi.org/10.3389/fnut.2022.1010005

[23] Wu, X., Song, M. Y., Qiu, P. J., et al. Discovery of anthocyanins from cranberry extract as pancreatic lipase inhibitors using a combined approach of ultrafiltration, molecular simulation and spectroscopy. *Food & Function*, **2018**, 9: 87–95. https://doi.org/10.1039/C7FO01155E

[24] Silva, A. L. P., Nascimento, R. G., Arakaki, L. N. H., et al. Organofunctionalized silica gel as a support for lipase. *Journal of Non-Crystalline Solids*, **2013**, 376: 139–144. https://doi.org/10.1016/j.jnoncrysol.2013.05.026

[25] Hakiminia, F., Ranjbar, B., Khalifeh, K., et al. Kinetic and thermodynamic properties of *pseudomonas fluorescence* lipase upon addition of proline. *International Journal of Biological Macromolecules*, **2013**, 55: 123–126. https://doi.org/10.1016/j.ijbiomac.2012.12.046

[26] Cheng, G. R., Pi, Z. F., Zheng, Z., et al. Magnetic nanoparticles-based lactate dehydrogenase microreactor as a drug discovery tool for rapid screening inhibitors from natural products. *Talanta*, **2020**, 209: 120554. https://doi.org/10.1016/j.talanta.2019.120554

[27] Poonsin, T., Simpson, B. K., Visessanguan, W., et al. Optimal immobilization of trypsin from the spleen of albacore tuna (*Thunnus alalunga*) and its characterization. *International Journal of Biological Macromolecules*, **2020**, 143: 462–471. https://doi.org/10.1016/j.ijbiomac.2019.10.030

[28] Nadar, S. S., Vaidya, L., Rathod, V. K. Enzyme embedded metal organic framework (enzyme–MOF): *de novo* approaches for immobilization. *International Journal of Biological Macromolecules*, **2020**, 149: 861–876. https://doi.org/10.1016/j.ijbiomac.2020.01.240

[29] Chen, H., Ouyang, K. H., Jiang, Y., et al. Constituent analysis of the ethanol extracts of *Chimonanthus nitens* Oliv. leaves and their inhibitory effect on *α*-glucosidase activity. *International Journal of Biological Macromolecules*, **2017**, 98: 829–836. https://doi.org/10.1016/j.ijbiomac.2017.02.044

[30] Yang, J., Qian, D. W., Jiang, S., et al. Identification of rutin deglycosylated metabolites produced by human intestinal bacteria using UPLC–Q-TOF/MS. *Journal of Chromatography B*, **2012**, 898: 95–100. https://doi.org/10.1016/j.jchromb.2012.04.024

[31] Li, A. X., Hou, X. C., Wei, Y. Fast screening of flavonoids from switchgrass and *Mikania micrantha* by liquid chromatography hybrid-ion trap time-of-flight mass spectrometry. *Analytical Methods*, **2018**, 10: 109–122. https://doi.org/10.1039/C7AY02103H

[32] Zeng, F., Wu, W. X., Zhang, Y. Y., et al. Rapid screening of lipase inhibitors in licorice extract by using porcine pancreatic lipase immobilized on Fe_3O_4 magnetic nanoparticles. *Food & Function*, **2021**, 12: 5650–5657. https://doi.org/10.1039/D0FO03352A

[33] Yang, F., Zou, Y. F., Li, C. Y., et al. Discovery of potential hypoglycemic metabolites in Cassiae Semen by coupling UHPLC-QTOF-MS/MS combined plant metabolomics and spectrum-effect relationship analyses. *Food & Function*, **2022**, 13: 10291–10304. https://doi.org/10.1039/D2FO00562J

[34] Kumar, A., Chauhan, S. Pancreatic lipase inhibitors: the road voyaged and successes. *Life Sciences*, **2021**, 271: 119115. https://doi.org/10.1016/j.lfs.2021.119115

[35] Wang, J., Ge, W., Peng, X., et al. Investigating the active compounds and mechanism of HuaShi XuanFei formula for prevention and treatment of COVID-19 based on network pharmacology and molecular docking analysis. *Molecular Diversity*, **2022**, 26: 1175–1190. https://doi.org/10.1007/s11030-021-10244-0